Presented at the 4th Symposium on the Cerro Prieto Geothermal Field, Guadalajara, Mexico, August 10-12, 1982.

LBL-14897
CP-25

LBL--14897

DE83 009053

MODELING STUDIES ON CERRO PRIETO

DISCLAIMER

This report was prepared as an account of work sponsored by an agency of the United States Government. Neither the United States Government nor any agency thereof, nor any of their employees, makes any warranty, express or implied, or assumes any legal liability or responsibility for the accuracy, completeness, or usefulness of any information, apparatus, product, or process disclosed, or represents that its use would not infringe privately owned rights. Reference herein to any specific commercial product, process, or service by trade name, trademark, manufacturer, or otherwise does not necessarily constitute or imply its endorsement, recommendation, or favoring by the United States Government or any agency thereof. The views and opinions of authors expressed herein do not necessarily state or reflect those of the United States Government or any agency thereof.

by

M. J. Lippmann and G. S. Bodvarsson

Earth Sciences Division
Lawrence Berkeley Laboratory
University of California
Berkeley, California 94720

NOTICE
PORTIONS OF THIS REPORT ARE ILLEGIBLE.
It has been reproduced from the best available copy to permit the broadest possible availability.

October 1982

This work was supported by the Assitant Secretary for Conservation and Renewable Energy, Office of Renewable Technology, Division of Geothermal and Hydropower Technologies of the U.S. Department of Energy under Contract No. DE-AC03-76SF00098.

MASTER

DISTRIBUTION OF THIS DOCUMENT IS UNLIMITED

DISCLAIMER

This report was prepared as an account of work sponsored by an agency of the United States Government. Neither the United States Government nor any agency Thereof, nor any of their employees, makes any warranty, express or implied, or assumes any legal liability or responsibility for the accuracy, completeness, or usefulness of any information, apparatus, product, or process disclosed, or represents that its use would not infringe privately owned rights. Reference herein to any specific commercial product, process, or service by trade name, trademark, manufacturer, or otherwise does not necessarily constitute or imply its endorsement, recommendation, or favoring by the United States Government or any agency thereof. The views and opinions of authors expressed herein do not necessarily state or reflect those of the United States Government or any agency thereof.

DISCLAIMER

Portions of this document may be illegible in electronic image products. Images are produced from the best available original document.

MODELING STUDIES ON CERRO PRIETO

M. J. Lippmann and G. S. Bodvarsson
Lawrence Berkeley Laboratory, University of California
Berkeley, California 94720

ABSTRACT

Numerical simulation techniques are employed in studies of the natural flow of heat and mass through the Cerro Prieto reservoir and of the effects of exploitation on the field's behavior. We consider a two-dimensional reservoir model that is based on the hydrogeologic model of Halfman et al. (this volume). The numerical code MULKOM is used in the simulation studies.

In the simulations of the natural state of the Cerro Prieto system, we employ five models that differ in prescribed material properties, boundary conditions, or geologic features. For each of these models we compute the steady-state pressure and temperature distributions and compare them against known preproduction pressures and temperatures. A good match between observed and calculated temperature and pressure distributions was obtained, and a natural hot-water flow rate of about 10^{-2} kg/s·m through the geothermal system was calculated.

The models are then used to simulate the behavior of the field under exploitation during the years 1973-1978. An acceptable match of temperature and pressure changes in the producing reservoir was obtained. The resulting flow patterns illustrate the effects of cold water recharge, boiling zones and hot fluid flow from depth on the overall field performance. The fluid recharge patterns agree with some of those postulated in earlier studies.

INTRODUCTION

The Cerro Prieto geothermal field is a complex geological and hydrological system. The natural flows through the geothermal reservoirs are controlled by layered sedimentary units (sands and shales), major faults zones, bouyancy effects and the regional hydrological pressure gradient. All of these factors must be considered in modeling the Cerro Prieto reservoirs.

Several authors have presented generalized models describing the natural (initial) conditions of the Cerro Prieto field and its evolution under production. A model for the natural flow pattern in the Cerro Prieto system was initially suggested by Mercado (1976) using geochemical data. Later, Elders et al. (1981) used mineralogic and isotopic data from well cuttings and cores to develop flow patterns for the field in its natural state. Both models show similar characteristics. The heat source for the hydrothermal system is located to the east. A plume of hot water ascends from the source, boiling as it rises, discharging upwards and horizontally to the west forming hot springs and fumaroles at the surface.

Both models indicate that cold water recharges the system through shallow layers from the east. However, Mercado (1976) also postulates cold water entering the field from the west. Elders et al. (1981) using isotope data and fission track data estimated an average velocity of 6 m/yr for the rising plume of hot fluids.

The general dynamics of the α (shallow) reservoir were described by Grant et al. (1981) based on chemical, production and reservoir engineering data. They concluded that the reservoir is bounded below by low-permeability rocks, and above and at the sides by zones of cooler waters. There seem to be no continuous permeability barriers around or immediately above the reservoir. The dominating cooling process in the natural state is mixing of hot reservoir fluids with colder surrounding fluids. Exploitation causes displacement of hot water by cooler water, and consequently, the reservoir temperatures tend to decline. Local boiling occurs near most wells in response to pressure decreases, but there is no indication that a continuous two-phase zone has formed in the reservoir.

Recently, Halfman et al. (this volume) have developed a hydrogeological model of the Cerro Prieto system based on well log and reservoir engineering data. They identify permeable and less permeable zones, and postulate the flow of geothermal fluids in the reservoir. The fluid flow patterns in a southwest-northeast section (Figure 1) are similar to those suggested by Mercado (1976) and Elders et al. (1981). Halfman's model, however, is much more detailed with respect to depths and location of the geothermal aquifers.

METHODOLOGY

In the above models, the mass and energy transport in the Cerro Prieto reservoirs have not been quantified. In the present work we employ numerical techniques to estimate the natural fluid flows through the reservoirs using measured values of temperature and pressure at different depths as a basis for comparison. We then use the models developed for the natural state of the reservoir to examine phenomena that occur during exploitation. The effects of exploitation on pressure and temperature decline, the rate of recharge of cold water, and the extent of the two-phase zone in the reservoir are considered.

RESERVOIR MODEL

We have developed a two-dimensional reservoir model, based on Halfman's hydrogeologic model, for the numerical simulation studies (Figure 2). The locations of three selected wells are shown in Figure 2 for comparison with the cross-section shown in Figure 1. The grid blocks used in the

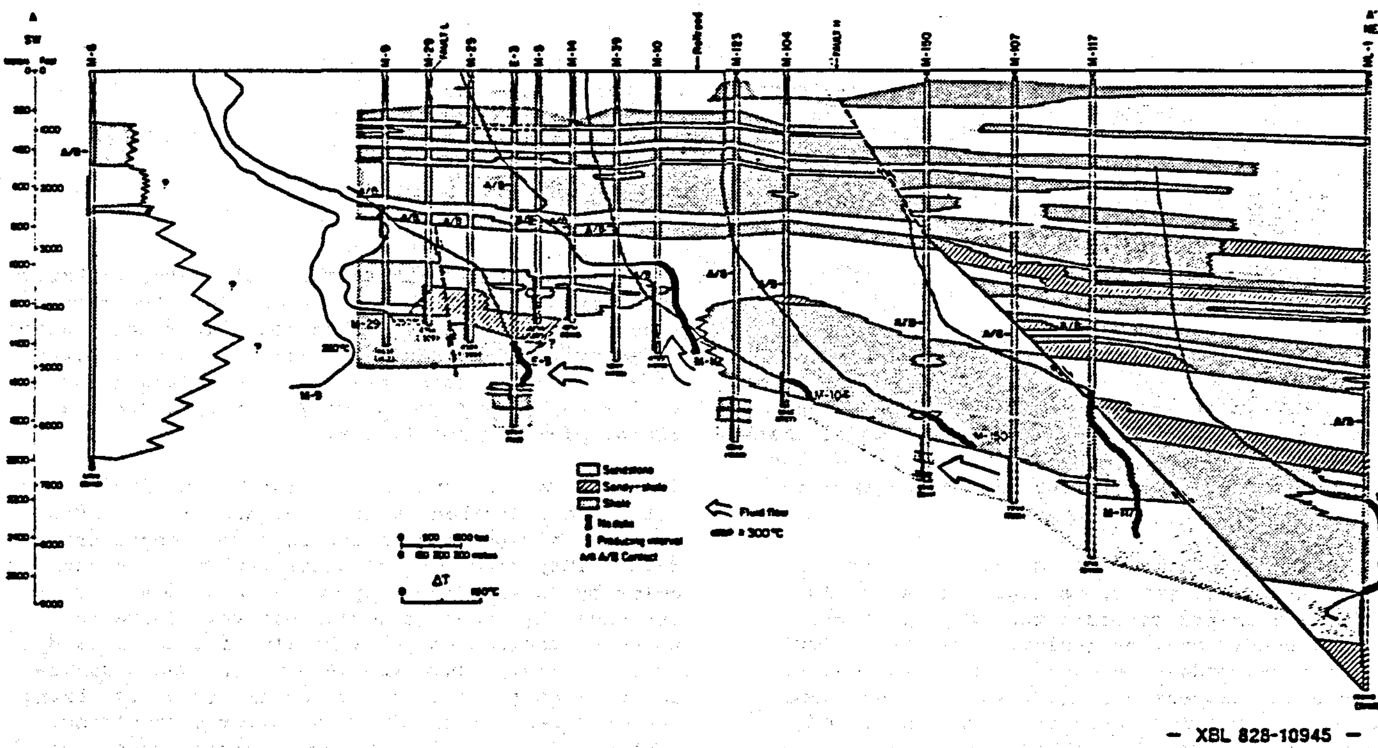

Figure 1. Southwest-northeast cross-section of the Cerro Prieto field showing schematically the flow of geothermal fluids in the system (from Halfman et al., this volume).

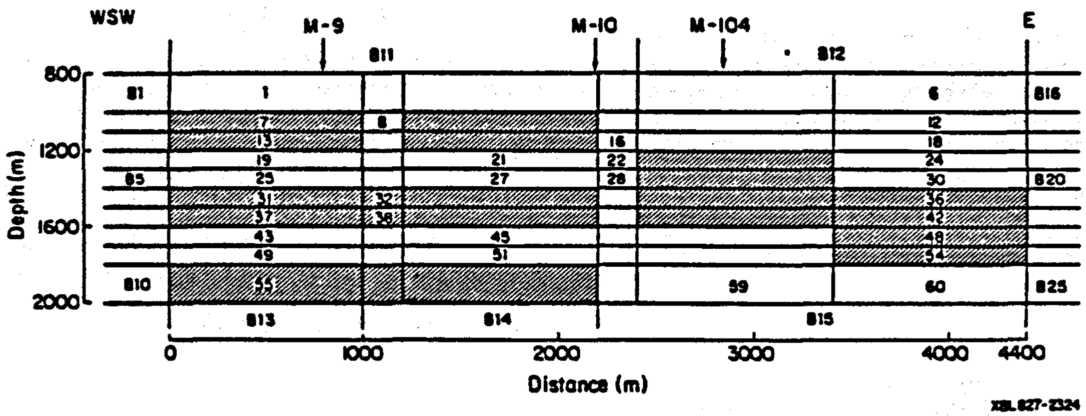

Figure 2. Two dimensional model of the field used in this work. Grid blocks, grid block numbers, and location of three wells are shown. The hatched zones indicate layers of lower permeability.

simulations are also shown in Figure 2; the hatched zones indicating layers of lower permeability. The mesh consists of 60 "internal" elements and 25 boundary elements. The flow region modeled extends from east to west-southwest at a depth of 800-2000 meters, and with a thickness of 1 meter.

The elements in the mesh can be grouped into different zones depending upon their material properties (Figure 3). The "S1" zone corresponds to the cooler aquifer overlying the main geothermal reservoirs in the western region. In the same region, the "C1" zone represents the shaly layer above the α reservoir (zone "S2"). The shaly zone "C2" separates in the western region the α and β reservoirs, the latter represented by the zone "S3". The zone "C3" is a low-permeability layer underlying the β reservoir. The zone "F" represents a fault zone that is postulated between wells M-25 and M-29.

In the eastern region, the "S4" zone represents a thick sandy unit overlying the thick shaly "C4" zone. Underlying the latter zone there is the sandy zone "S5" which corresponds to the eastern portion of the β reservoir which extends upwards communicating with the sandy zones "S2" and "S3".

The zone "C5" represents a region of low-permeability assumed to be formed by the precipitation of calcite as cooler water comes in contact with hotter rocks.

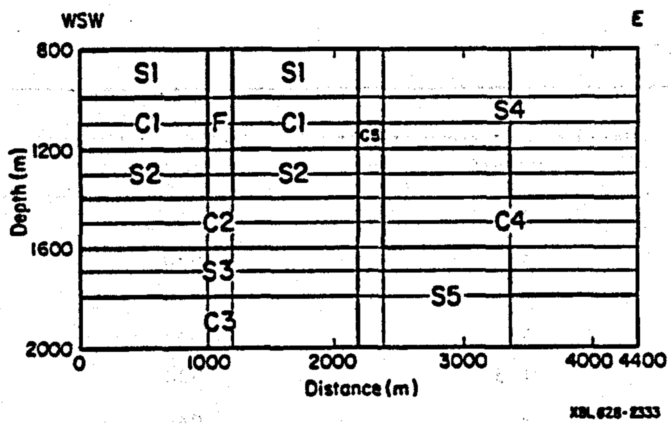

Figure 3. Different zones used in the model.

As will be discussed below, the material properties and geometry of some of these zones were changed in some cases so as to obtain a better match between observed and calculated pressures and temperatures.

ROCK PROPERTIES

For the simulation studies, the single most important reservoir parameter is its permeability. Analysis of well test data indicates that the permeability of the Cerro Prieto reservoirs lies in the range of tens to a few hundred millidarcies (Schroeder et al., 1978; Rivera et al., 1978; Abril and Vargas, 1981).

Values of transmissivity reported by the same authors vary between 3.6 and 40 darcy-meters. On the other hand, laboratory core analysis give permeabilities of tenths or few millidarcies (Abou-Sayed et al., 1979; Schatz, 1981) possibly because their measurements indicate vertical permeabilities obtained along the axis of the cores. No measurements have been made on relative permeabilities of Cerro Prieto rocks.

Rock porosity, compressibility, heat conductivity and heat capacity data are also needed for simulation studies, although the effects of these parameters are not as great as those of permeability.

A number of authors have presented data on porosity (Martínez, 1978; Abou-Sayed et al., 1979; Lyons and van de Kamp, 1980; Schatz, 1981); the values reported vary between 4 and 39%. The porosity does not only depend on the rock type, but also changes with depth.

Measurements of deformation properties of Cerro Prieto cores were made by Somerton (1978), Abou-Sayed et al. (1979) and Schatz (1981). These studies indicate that the rock compressiblity is on the order of 10^{-10} Pa^{-1}. Martínez (1978) measured thermal conductivities of Cerro Prieto rocks obtaining values between 0.5 and 4.6 W/m°C for sandstones, and between 1.4 and 3.1 W/m°C for shales and silts. No measurements have been made on the heat capacities of these rocks.

In the present simulation studies, seven different materials were used (Table 1). These materials differ mainly in permeability, with only slight variations in density, thermal conductivity and heat capacity. The rock porosity and compressibility was assumed to be the same for all materials or 20% and 5×10^{-10} Pa^{-1}, respectively. The interrelations between the different zones in the model and the different materials are given in Table 2. One should note that the permeability of most of the materials is assumed anisotropic because of the layered nature of the sediments at Cerro Prieto. All of the zones shown in Figure 3 consist of shale and sand sequences in different proportions. The only material which was assumed to be isotropic is material 4 which represents the fault zone located between wells M-25 and M-29.

Relative permeabilities of the two-phase (liquid and vapor) zones were calculated using the Corey curves. In functional form, these curves are represented by the following equations:

$$k_{rl} = \begin{cases} [S^*]^4 & S < S_{rl} \\ 0 & S \geq S_{rl} \end{cases} \quad (1)$$

$$k_{rv} = \begin{cases} [1 - S^*]^2[1 - (S^*)^2] & S > S_{rv} \\ 0 & S \leq S_{rv} \end{cases} \quad (2)$$

$$\text{where} \quad S^* = \frac{1 - S_{rl} - S}{1 - S_{rl} - S_{rv}} .$$

All of the symbols are defined in the nomenclature. In the present work we used $S_{rl} = 0.30$ and $S_{rv} = 0.05$.

TEMPERATURE AND PRESSURE MEASUREMENTS

The temperature distribution of the western portion of the Cerro Prieto field in its natural state is given by Mercado (1976) (Figure 4). Recently, Castillo et al. (1981) presented the temperature distribution in the eastern portion of the field; the reported temperature distribution may have been affected by the exploitation of the western area. During exploitation, wells at Cerro Prieto have shown a decline in temperature of the produced fluids. Fausto et al. (1981) and Grant et al. (1981) show, for selected wells, temperature changes with time based on the Na-K-Ca geothermometer (Figure 5).

Castillo et al. (1981) present temperature data for the eastern part of the deeper β reservoir. Detailed maps showing the temperature distribution in the western part of this reservoir have not yet been published.

Pre-exploitation pressures in the α reservoir (1200 m depth) are shown in Figure 6 (mid-1973 data) and Figure 7 shows the pressure contours at the same datum in 1979 (Bermejo et al., 1979). The pressure decline in the α reservoir with time is shown in Figures 8 and 9 (Bermejo et al., 1979).

Table 1. Properties of the materials used in the models.

Material	Rock density (kg/cm^3)	Permeability Horizontal (md)	Permeability Vertical (md)	Matrix Heat conductivity (W/m°C)	Rock Heat Capacity (J/kg°C)
1	2650	100	1	3	820
2	2650	10	1	3	820
3	2550	0.5	0.005	2	920
4	2650	50	50	3	820
5	2700	0.05	0.005	1.5	920
6	2650	100	10	3	820
7	2550	1	0.1	2.5	920

Table 2. Material assigned to the zones shown in Figure 3.

Zone	Material
S1	6
S2	6
S3	6
S4	2
S5	1
F	4
C1	7
C2	7
C3	5
C4	3
C5	3

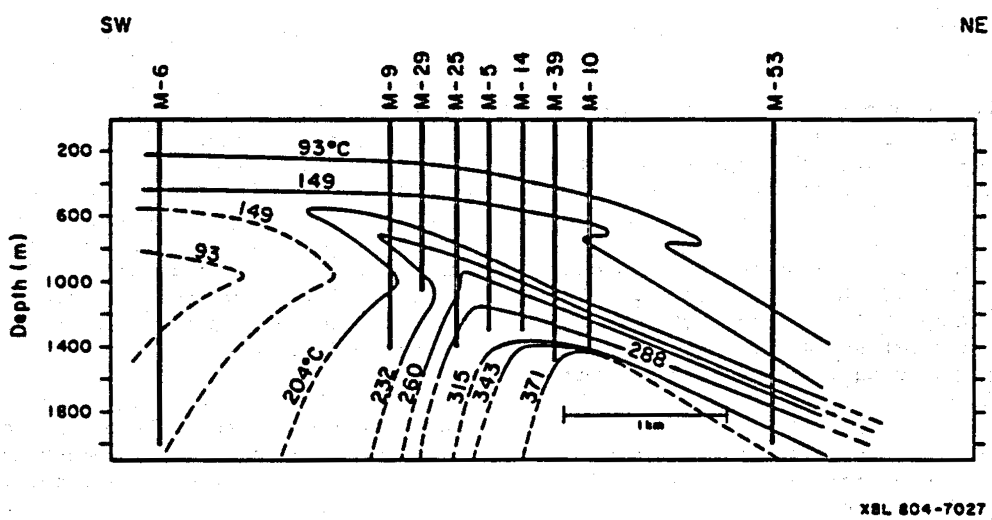

Figure 4. Preproduction temperature distribution in the Cerro Prieto field along a southwest-northeast cross-section (adapted from Mercado, 1976).

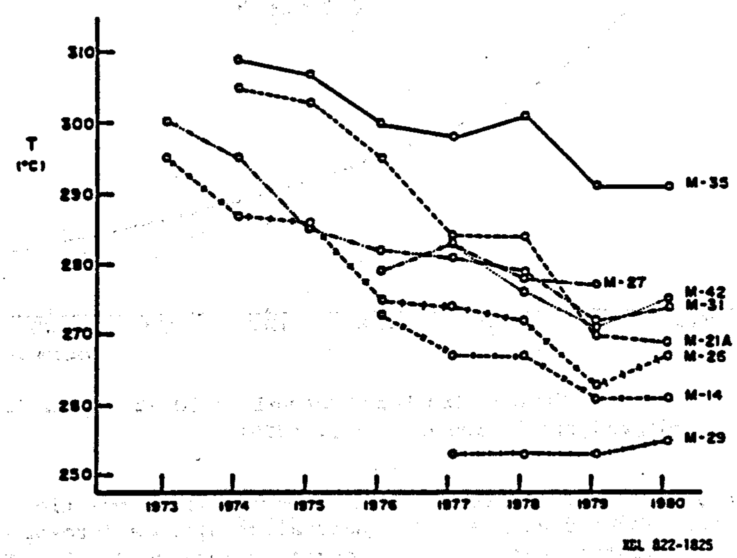

Figure 5. Changes in the Na-K-Ca temperatures in some Cerro Prieto wells (from Fausto et al., 1981).

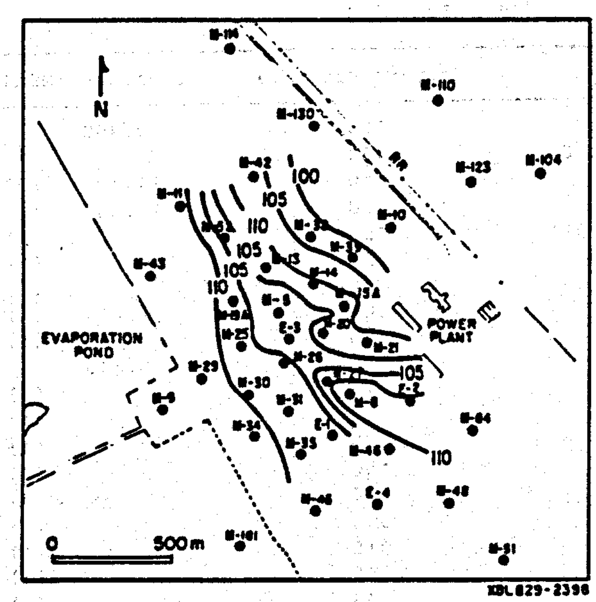

Figure 6. 1973 pressures (in bars) in the α reservoir, at 1200 m depth (adapted from Bermejo et al., 1979).

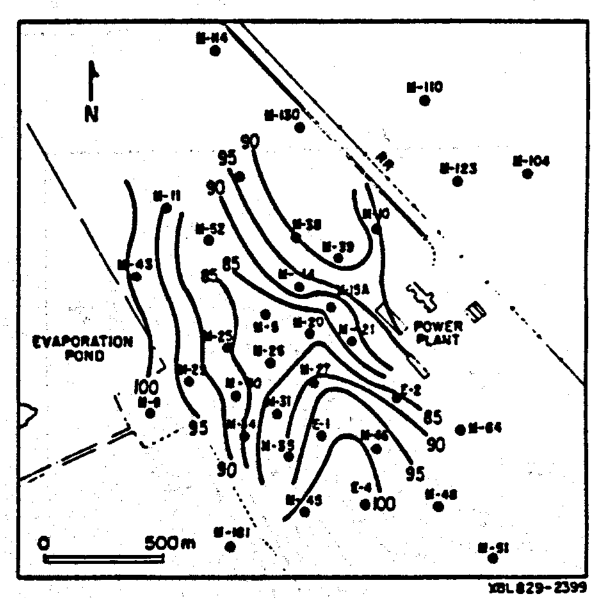

Figure 7. 1979 pressures (in bars) in the α reservoir, at 1200 m depth (adapted from Bermejo et al., 1979).

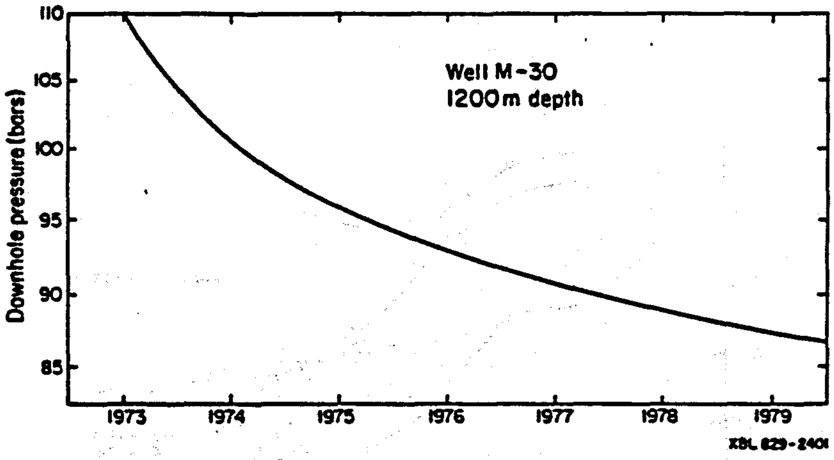

Figure 8. Pressure changes (in bars) in well M-30 at 1200 m depth (adapted from Bermejo et al., 1979).

Limited data have been published on the pressure distribution in the β reservoir. Sánchez and de la Peña (1981) give a partial piezometric map for this reservoir.

BOUNDARY CONDITIONS

The boundary nodes, nodes B1 to B25 in Figure 2, have constant temperatures and pressures. All of them are open to heat flow, but only selected ones are open to fluid flow. The temperatures of the boundary nodes were varied to some degree until a reasonable match between observed and calculated temperature data was obtained. The best match was obtained when the values given in Table 3 were used.

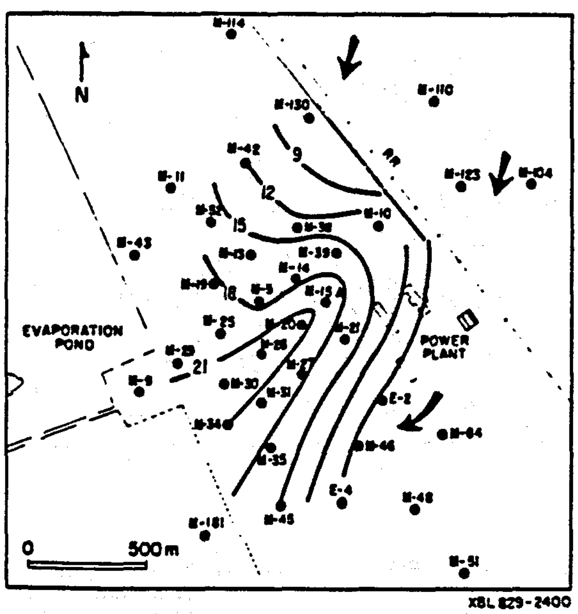

Figure 9. Pressure changes (in bars) in the α reservoir from 1973 to 1979 (at 1200 m depth) and postulated direction of fluid recharge (adapted from Bermejo et al., 1979.

During the simulations of the system under natural conditions (pre-production), only the boundary elements B1, B4, B5, B16 and B25 were assumed open to fluid flow. The pressure in these nodes was calculated based on the average fluid density of the overlying fluids and the depth to the midpoint of the boundary node. The values used are given in Table 3. The pressure in element B25 was adjusted during the simulations until a reasonable match with observed pressure and temperature data was obtained.

Table 3. Constant temperature and pressure at boundary nodes.

Node	Temperature (°C)	Pressure (MPa)
B1	220	8.300
B2 and B3	150	(1)
B4	150	11.523 (2)
B5	150	12.445 (2)
B6 to B11	150	(1)
B12	50	(1)
B13	230	(1)
B14	300	(1)
B15	360	(1)
B16	50	8.815
B17	75	(1)
B18	100	(1)
B19	125	(1)
B20	150	(1)
B21	250	(1)
B22	300	(1)
B23	315	(1)
B24	340	(1)
B25	355	(3)

(1) These nodes were assumed to be closed to fluid flow while modelling the natural state considering that they were in pressure equilibrium with the internal part of the system. When fluid production was simulated, it was assumed that the pressures in these boundary nodes were equal to the initial pressures of the neighboring internal nodes.

(2) In case 4, these pressures were changed to 11.278 MPa (node B4) and 12.180 MPa (node B5).

(3) The pressure in node B25 was adjusted to allow the inflow of about 10^{-2} kg/s·m of 355°C water.

Later, while modeling the field under production, all lateral boundary nodes (B1 to B10, and B16 to B25) were assumed to have constant pressures and be open to fluid flow. The pressures assigned to the nodes were equal to those corresponding to the natural state.

COMPUTER MODEL

In this study, the three-dimensional, multiphase, multi-component simulator MULKOM was used. MULKOM was developed by K. Pruess at Lawrence Berkeley Laboratory for modeling the flow of water/steam mixtures and heat in porous or fractured rock masses. The thermophysical properties of water are accurately represented by the steam table equations given by the International Formulation Committee (1967). MULKOM is an advanced version of the geothermal reservoir simulator SHAFT79 (Pruess and Schroeder, 1980), which has been extensively validated both analytically and numerically (Stanford University, 1980).

MODEL STUDIES

In the present work we employ numerical methods to study mass and heat flow through the Cerro Prieto system in its natural state and the effects of exploitation on the pressures, temperatures and boiling in the system. By employing a two-dimensional model, we make the important assumption that the mass and energy fluxes in the third dimension are negligible. In the case of natural flows, we believe that this approximation is quite reasonable, as the model is oriented in the direction of the primary flow components, inferred from Halfman et al's well log studies (this volume). However, in studies of the behavior of the field under exploitation, the two-dimensional assumption becomes much more critical. Massive exploitation will invariably lead to three-dimensional flow patterns. Therefore, the studies of the reservoir behavior during exploitation can only yield qualitative results.

MODELING OF THE NATURAL STATE

We assume that the field is under steady-state conditions in its natural state. We thus neglect the very slow temporal changes in the thermal or fluid flow regime that have been suggested by some mineralogic studies (Elders et al., 1981). The initial thermodynamic conditions in the models used for the natural-state computations were assumed to depend only on depth. The temperature and pressure increased linearly with depth, with single-phase liquid conditions everywhere. Steady-state conditions were generally reached after 10-100 thousand years of simulation.

Five models simulating the natural mass and heat flows in the Cerro Prieto geothermal system are considered. In a general sense, all of the models are quite similar, but the slight differences give important insight into how the material properties, the boundary conditions and certain geologic features affect the steady-state mass and heat flows in the system. We will first explain the general physical processes that the models exhibit and then discuss results from simulations using individual models.

The basic model considered represents the geologic formations between 800 and 2000 m depth, as shown schematically in Figure 2. At the top of the model (800-1000 m depth), there is a shallow cooler aquifer which extends all across the system (zones S1 and S4, Figure 3) and which is assumed to be overlain by an impermeable layer at 800 m depth. Cold (50°C) water is recharging this aquifer from the east (through node B16, Figure 2). Hot (about 240°C) water is flowing into this aquifer from depth through the fault zone (zone F) located between wells M-25 and M-29 (node 8). This shallow aquifer discharges fluids to the west (through node B1) feeding the surface manifestations that are observed in that area. It is assumed that the western part of the aquifer is more permeable than the eastern part.

In the western part, a permeable shaly layer (zone C1) separates the shallow cooler aquifer from the α reservoir (1200-1400 m depth). As mentioned earlier, this shaly layer is cut by the fault between M-25 and M-29 (zone F) which allows the upward movement of hot fluids.

Below this shaly layer the α reservoir (zone S2) is recharged from the east with hot waters which ascend through the vertical gap existing between the shaly layers east of well M-10 (Figure 1). Cooler waters (150°C) recharge the α reservoir from the west. Under natural conditions both hot and cold water move towards the fault zone, and then upwards along the fault zone.

In the western region the α reservoir is separated from the deeper β reservoir (zone S3) by a continuous but leaky shaly layer (zone C2). We assume that the fault zone has been sealed by mineral deposition between 1400 and 1600 m depth, so that it does not allow rapid transport of hot water to the α reservoir. In the western part of the system we assume that this reservoir is in hydraulic equilibrium with colder (150°C) waters.

A low-permeability, low-conductivity layer (zone C3) is assumed to underlie the β reservoir. Because of the lower temperature prevailing in boundary nodes B13 and B14 (Table 3), there is a decrease of temperature with depth, as observed in the western region below the β reservoir.

In the eastern region below the cold shallow aquifer discussed earlier, there is a thick shaly, low-permeability unit (zone C4) which acts as a confining layer to the underlying β reservoir (zone S5). The depth to the β reservoir increases towards the east where it is recharged with 355°C liquid water (through node B25). This fluid is believed to be heated at depth by a swarm of intruded dikes (W. Elders, 1982, personal communication).

The vertical gap between the shaly units (Figure 1, east of well M-10) could allow fluid flow between the shallow cold aquifer and the geothermal reservoirs. If the vertical permeability of the sandy materials in this gap is high, the cold water moves downward because of its higher density and gradually cools the geothermal resource.

The vertical permeability of the sandy materials in this gap is probably not very large because the hot water as it rises through the gap, tends to precipitate minerals as it boils (Elders et al., 1981).

We consider that the fluid flow between the shallow aquifer (zones S1 and S4) and the geothermal system below was restricted by the existence of a low-permeability zone (zone C5, node 16) created by the self-sealing of the sediments as the cold recharge water is heated (Elders et al., 1981).

MODEL 1

The materials assigned to the various zones of Model 1 are those given in Table 2. The boundary conditions used are described in Table 3.

Figures 10 and 11 show the steady-state temperature distribution and fluid flow pattern in the system. The hatched regions represent the lower permeability zones and the dotted regions the areas where boiling occurs. Some of the results obtained in this model are summarized in Table 4.

The temperature of the α reservoir (nodes 21 and 27 in Figure 2) varies between 291 and 299°C. The pressure at 1250 m depth (node 21) is 11.52 MPa. At 1200 m it would be about 11.11 MPa, which compares well with the 1973 pressures shown in Figure 6.

The temperatures in nodes 45 and 51, representing the β reservoir in the western part, are 330 and 329°C, respectively. The pressure in node 51 (1750 m depth) is 15.93 MPa. This value is slightly higher than the pressure reported by Prian (1981) for well E-1 (15.30 MPa). However, the pressure in well E-1 was measured in January 1981 about two years after fluid extraction started in the β aquifer in the southwestern and eastern parts of the field.

Boiling is restricted to the eastern part of the field, in the upflow region and part of the β aquifer. The flow patterns shown in Figure 11 indicate a significant cold water recharge from the west and an even larger upward flow through the fault zone near M-29. The ascending water eventually discharges at the upper left corner of the model.

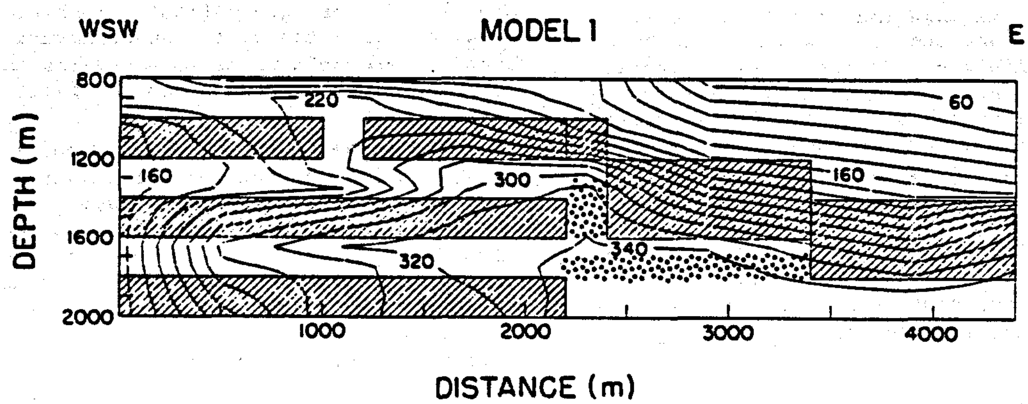

Figure 10. Model 1 - Natural state. Steady-state temperature distribution; contour interval: 20°C. Hatched areas represent layers of lower permeability; dotted areas, two-phase zones.

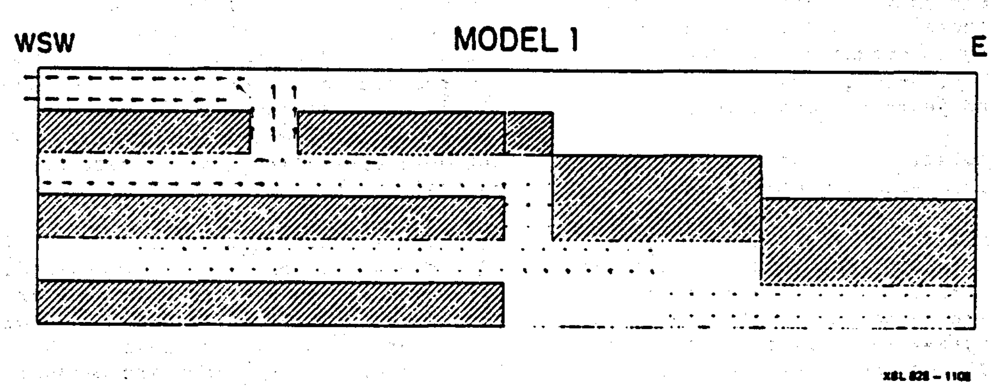

Figure 11. Model 1 - Natural state. Steady-state mass flow pattern. Length of arrows is scaled with respect to the largest flow rate (in kg/s·m^2).

Table 4. Natural State - Summary of Results

		Models				
		1	2	3	4	5
AQUIFER α						
Node 21	Temperature (°C)	291.0	297.3	267.3	297.0	288.9
	Pressure (MPa)	11.52	11.52	11.48	11.33	11.52
Node 27	Temperature (°C)	298.6	302.5	279.9	307.8	299.1
	Pressure (MPa)	12.24	12.24	12.24	12.04	12.25
Fluid Velocity (m/yr)						
Between Nodes 21-22		0.4	0.7	0.3	0.3	0.5
Between Nodes 27-28		1.4	3.5	0.5	1.5	1.6
AQUIFER β						
Node 45	Temperature (°C)	329.9	293.0	325.9	332.2	329.2
	Pressure (MPa)	15.28	16.83	14.53	15.06	15.27
Node 51	Temperature (°C)	328.8	285.4	323.7	331.3	328.3
	Pressure (MPa)	15.93	17.57	15.19	15.70	15.92
Node 59	Temperature (°C)	351.7	352.8	349.9	351.4	351.6
	Pressure (MPa)	17.06	18.61	16.52	16.86	17.05
Steam Saturation		0	0	0.14	0	0
BOUNDARIES						
Node 60	Influx of 355°C water (kg/s)	1.01×10^{-2}	1.03×10^{-2}	1.02×10^{-2}	1.02×10^{-2}	1.02×10^{-2}
Node 19	Influx of 150°C water (kg/s)	3.65×10^{-3}	4.49×10^{-3}	4.75×10^{-3}	8.84×10^{-4}	3.55×10^{-3}
Node 25	Influx of 150°C water (kg/s)	7.88×10^{-3}	7.57×10^{-3}	8.07×10^{-3}	5.42×10^{-3}	7.78×10^{-3}
Node 6	Influx of 50°C water (kg/s)	1.18×10^{-3}	9.87×10^{-4}	1.24×10^{-3}	1.41×10^{-3}	1.33×10^{-3}
Node 1	Outflow of hot water (kg/s)	2.28×10^{-2}	2.34×10^{-2}	2.43×10^{-2}	1.79×10^{-2}	2.28×10^{-2}
Node 1	Temperature (°C)	213.3	214.7	216.6	226.3	213.7

In the western part of the β reservoir some hot water enters from the east, part of which leaks upwards through the confining layer, while some moves westward where it cools in a not very well-defined convection cell. In the α reservoir east of the fault zone, the major component of flow is to the west, a small amount of colder water flows to the east in the lower part of the reservoir. Both waters mix and flow upwards through the fault.

In Figure 11 and other later figures, the length of the arrows is scaled with respect to the largest flow rate. Consequently, in regions where the flow is small, no arrows are present. The rates of fluid recharge and discharge, and the velocities in the α reservoir are given in Table 4.

MODEL 2

The only difference between Models 1 and 2 is that in the latter, the permeability of the shaly layer (zone C2) is lowered by using material 3 instead of material 7. The lower vertical permeability significantly reduces the leakage of hot waters through that layer, thus decreasing the flow of hot water into the western region of the β reservoir. This results in a large reduction of temperature and subsequent increase of pressure in the β reservoir; 285°C and 17.57 MPa in node 51 (see Table 4 and Figure 12). On the other hand, the temperature in the α reservoir is slightly higher than it was in Model 1 (297°C in node 21 and 302°C in node 27).

In this model, the steady-state conditions show that boiling is restricted to the upper part of the upflow channel. The pattern of fluid movement is similar to that of Model 1 except that less hot water enters the western part of the β reservoir.

MODEL 3

Model 3 differs from Model 1 only in that the fault zone between well M-25 and M-29 is open in nodes 32 and 38, allowing a direct connection between the α and β reservoirs in the western region of the field (Figures 13 and 14).

This gap in the shaly zone C2 makes the steady-state temperatures and pressures in the α reservoir considerably lower than in Models 1 and 2 (see Table 4). In the β reservoir, the temperature is similar to that for Models 1 and 2, but the pressure is considerably lower or 15.19 MPa in node 51; this value is lower than the one measured in well E-1 in early 1981 (15.30 MPa).

Since the low temperature and pressure in the α reservoir and the low pressures in the western part of the β reservoir are not consistent with the measured data, this model is considered inadequate for describing the natural state of the Cerro Prieto system.

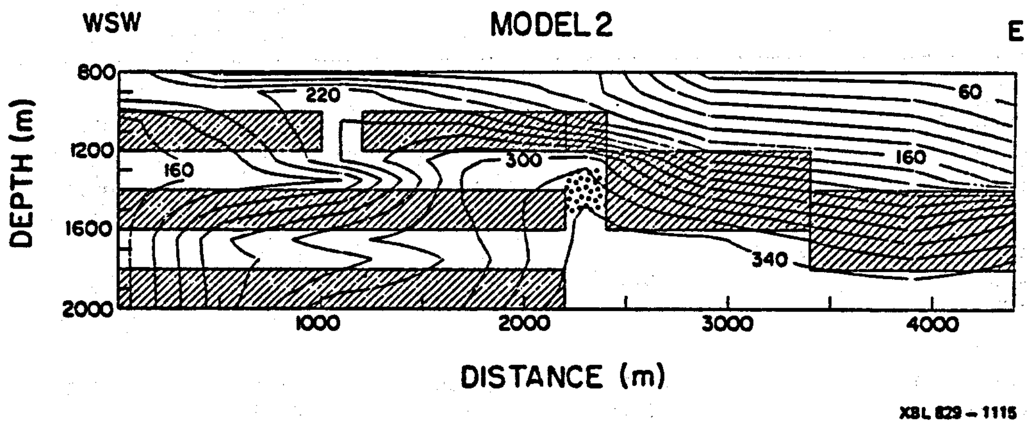

Figure 12. Model 2 - Natural state. Steady-state temperature distribution; contour interval: 20°C.

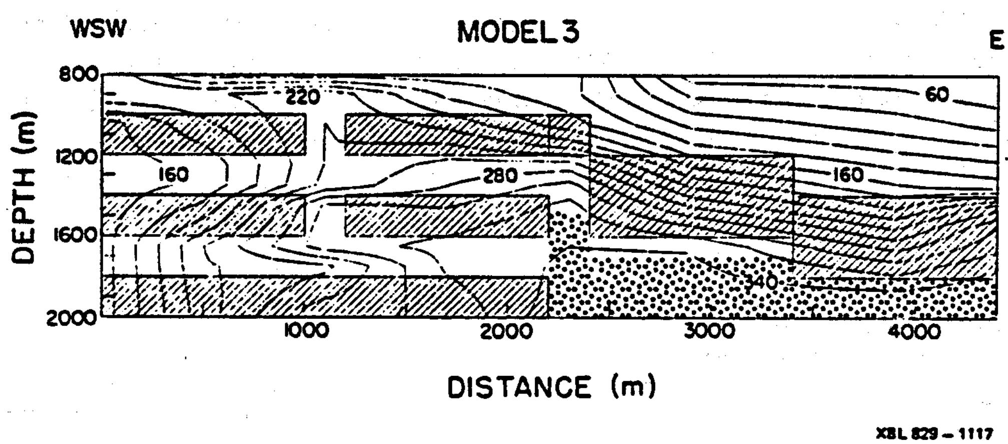

Figure 13. Model 3 - Natural state. Steady-state temperature distribution; contour interval: 20°C.

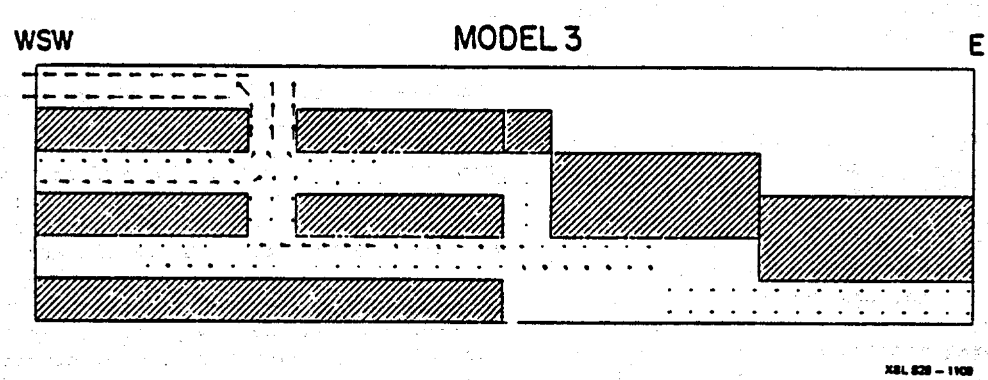

Figure 14. Model 3 - Natural state. Steady-state mass flow pattern.

MODEL 4

In Model 4, the pressures in boundary nodes B4 and B5 were decreased to 11.278 and 12.180 MPa, respectively. All other conditions in this model are the same as those of Model 1.

The reduction of pressure in these boundary nodes not only decreases the influx of the cooler (150°C) water into the α reservoir, but also reduces pressures throughout the system (Table 4). The temperature in the α reservoir rises to 297°C in node 21, and 308°C in node 27 (Figure 15). The pressure in node 21 is now 11.33 MPa, and at 1200 m depth it would be about 10.95 MPa, a value similar to those shown in Figure 6. The pressures and temperatures in the β reservoir are slightly lower than those in Model 1. This increases somewhat the extent of the boiling zone in the eastern regions of the β reservoir.

MODEL 5

In model 5, the material of node 16 (zone C5) is changed to Material 2; everything else is the same as in Model 1.

The higher permeability of the C5 zone, especially the vertical permeability, causes greater flows from the shallow cooler aquifer into the geothermal system. As expected, more colder water leaks into the upper zone of the ascending hot water plume resulting in a significant cooling of node 22, from 292°C in Model 1 to 254°C in Model 5. The rest of the system is only slightly affected (Table 4; Figures 16 and 17).

In additional simulations, the permeability of node 16, was increased even further, thus eliminating the self-sealing zone on top of the rising hot water plume, but the results showed even greater cooling of the α reservoir.

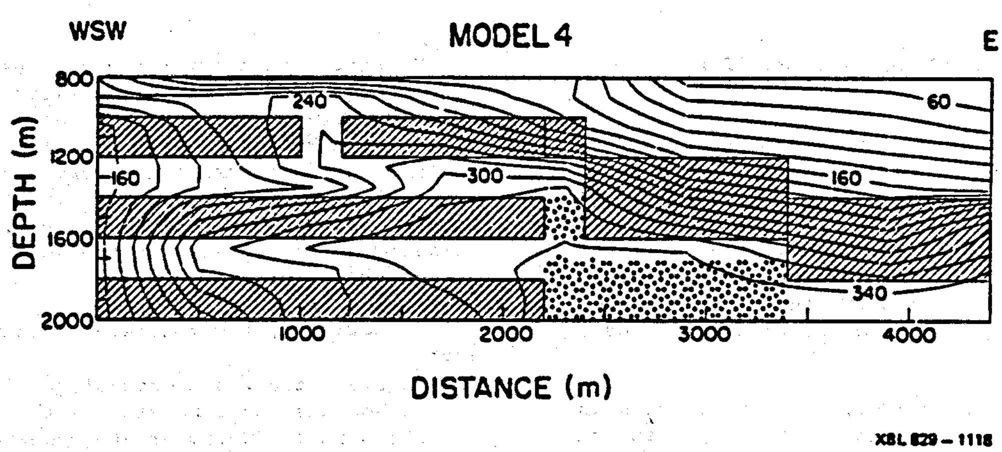

Figure 15. Model 4 - Natural state. Steady-state temperature distribution; contour interval: 20°C.

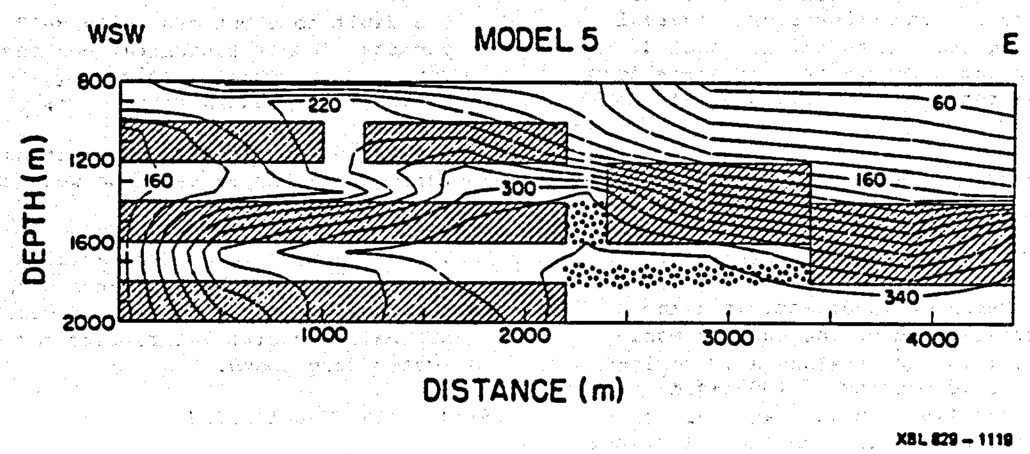

Figure 16. Model 5 - Natural state. Steady-state temperature distribution; contour interval: 20°C.

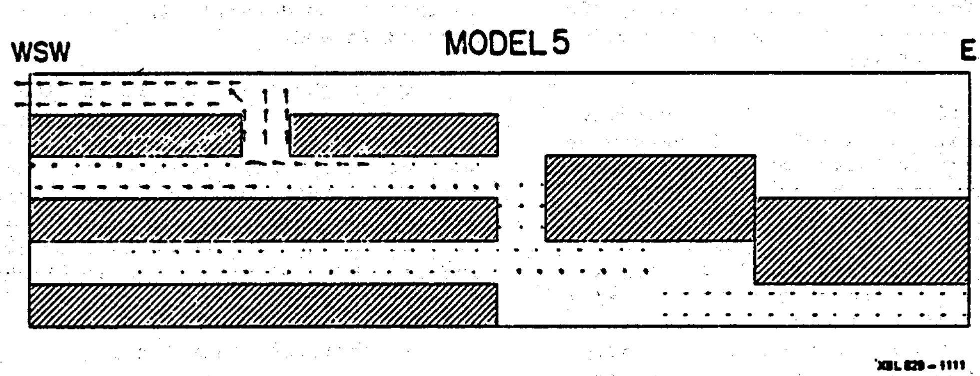

Figure 17. Model 5 - Natural state. Steady-state mass flow patterns.

DISCUSSION OF MODELS OF THE NATURAL STATE

In reviewing the results from different models tested (only a few are reported here), we feel that Models 1, 4 and 5 are those which best reproduce the initial distribution of temperatures and pressures in the field. Model 1 and 5 give somewhat higher pressures and lower temperatures in the system than Model 4 (Table 4), mainly because of larger influx of colder water into the α reservoir.

Model 5 gives relatively low temperatures in the upper eastern part of the α reservoir (in the region near M-10) which agree well with values reported by Mercado (1976) (see Figure 4).

Model 4 gives somewhat higher temperatures in the western region of the α reservoir in comparison with other models. These agree more closely to the temperatures given by Mercado (Figure 4) and also best reproduce the temperature reversal observed in that region. In addition, Model 4, gives pressures in the α reservoir that are almost identical to those reported by Bermejo et al. (1979) (Figure 6).

All five models give average fluid velocities in the α reservoir (Table 4) which are of the same order of magnitude as the one computed by Elders et al. (1981) for the hot plume (6 m/yr).

Furthermore, Mercado (1968) estimated the volume of the natural flows of the surface manifestations to be 5×10^6 m^3/yr along a 10 km long zone. Assuming a fluid density of 1000 kg/m^3, this outflow is about 1.6 kg x 10^{-2} kg/s·m. This value compares reasonably well with the calculated natural flow rates through the Cerro Prieto system. For example, the inflow of hot fluids into the β reservoir from the east (node 60) is about 1×10^{-2} kg/s·m, and the average outflow through node 1 is about 2×10^{-2} kg/s·m for the five models (Table 4).

We conducted a brief study to examine the effects of the relative permeability curves used on the steady-state temperature and pressure distribution in the Cerro Prieto system. We used linear relative permeability curves and compared the results to those obtained using the Corey curves. The results showed no significant differences, primarily because of the small extent of the two-phase zone.

Summarizing, the following conclusions can be made:

1. Halfman et al.'s hydrogeological model is reasonable and consistent with mass and heat flows in the Cerro Prieto reservoir;

2. The average natural rate of hot water recharge into the eastern part of the Cerro Prieto system is approximately 10^{-2} kg/s per meter of width (measured in a north-south direction);

3. The fault zone between wells M-25 and M-29 permits flow of fluids between the α reservoir and the shallow colder aquifer, but not between the α and β reservoirs;

4. The hot water plume boils as it ascends through the gap existing between the shaly layers;

5. There exists a lower permeability zone at the top of the vertical gap between the shaly layers which inhibits, or reduces, the influx of shallow cooler waters into the geothermal system from above.

SYSTEM UNDER EXPLOITATION

In the second part of the simulation studies, the models developed for the natural state were used to simulate the behavior of the Cerro Prieto system during exploitation. The purpose was to select the model which best reproduces the pressure and temperature changes in the α reservoir.

During exploitation we extract half of the fluid mass from node 21 and the other half from node 27 (see Figure 2): both nodes represent the main part of the α reservoir. The fluid production rates (Q_T) at the Cerro Prieto field between March 1973 and the end of 1979 are given in Table 5. Initially, these rates were divided by 1500 m (the approximate width of the production area in the western region) to take into consideration the two-dimensional nature of the models. This resulted in pressure drawdowns in the α reservoir (node 21) which were about twice as large as those reported by Bermejo et al. (1979). This discrepancy is caused mainly by the two-dimensional nature of the model, i.e. lack of recharge from the third dimension.

Several rate reductions were tested using model 5 and it was found that dividing the total rates (Q_T) by 3000 or 4000 m gave some relative agreement with the observed pressure changes (see Figure 18). The case for 3000 m gave a somewhat larger total pressure decline than what is observed, but the shape of the curve at later times fits the observed curve reasonably well. For the 4000 m case, the total drawdown is similar to the observed one, but the general shape of the pressure decline does not agree as well.

On the other hand, by studying the temperature changes in node 21 using different flow rates (Figure 19), it is clear that the 4000 m and 6000 m cases give too slow a temperature decline. The Na-K-Ca geothermometer indicates that between 1973 and 1978 the temperature in the α reservoir has dropped by up to 30°C (Figure 5). An average drop of 20°C over this period is a reasonable value (A. Truesdell, 1982, personal communication).

Based on the pressure and temperature response of Model 5, we decided to use the 3000 m width in all further simulations (i.e. $Q = Q_T/3000$ m).

Table 6 summarizes the temperature and pressure declines that were computed in the α reservoir (nodes 21 and 27).

Figure 20 shows the temperature versus time in node 21 for the five models. All the models show a temperature decline, as observed in the field, however, Model 3 shows too slow a temperature decline.

Table 5. Cerro Prieto Fluid Production.

Dates	Production Rates (kg/s)
3/73-12/73	459
1974	590
1975	603
1976	695
1977	751
1/78-6/78	671
7/78-12/78	761
1979	1210

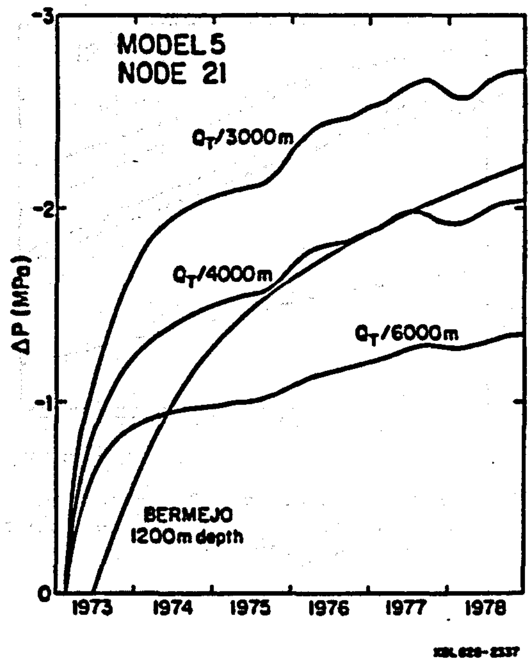

Figure 18. Model 5 - Exploitation. Pressure changes in node 21 under different production rates.

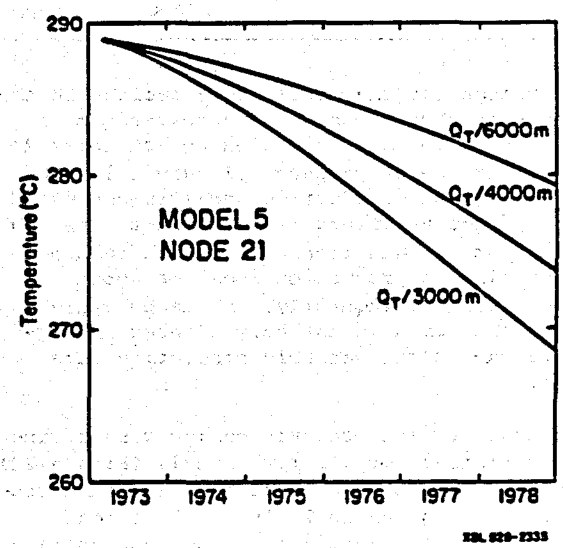

Figure 19. Model 5 - Exploitation. Temperature changes in node 21 under different production rates.

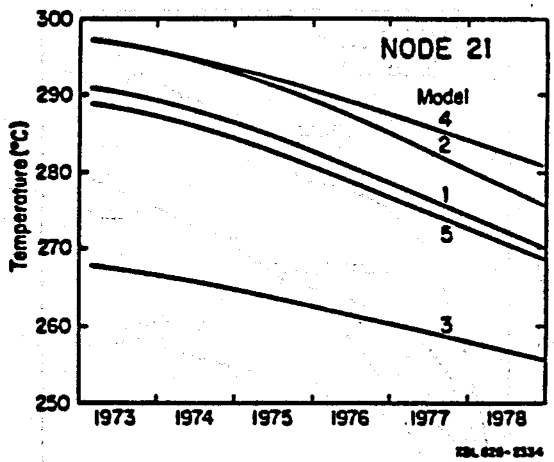

Figure 20. Temperature of node 21 versus time for the five models studied under exploitation ($Q = Q_T/3000$ m).

Table 6. Change of Temperature and Pressure in Nodes 21 and 27 (α reservoir) between March 1973 and December 1978.

	Node 21		Node 27	
	T (°C)	P (MPa)	T (°C)	P (MPa)
Model 1	-20.9	-2.78	-23.5	-2.76
Model 2	-21.8	-2.97	-29.1	-2.95
Model 3	-12.0	-2.29	- 8.6	-2.27
Model 4	-16.6	-2.60	-21.4	-2.57
Model 5	-20.4	-2.71	-23.5	-2.69

The reason for the temperature decline in the α reservoir is obvious when one compares the energy inflow into the production nodes (nodes 21 and 27) to the energy produced (Figure 21). The fluid flow into the production nodes is dominated by inflow of cooler waters from the west. The low energy content of this recharge results in a net energy loss in the production nodes of about 0.5×10^5 J/s.m; consequently, the temperature declines. The bumps in the curves shown in Figure 21 are due to the variable production rate (Table 5).

The shape of the pressure change versus time curves are similar for all five models (Figure 22). The bumps in the curves are due to changes in production rate, as given in Table 5. Some models seem to react less abruptly to these changes (e.g., Models 1 and 4) possibly because of somewhat higher overall compressibility of the α reservoir.

The shape of these curves shows that soon after a change in the production rate occurs, the pressure tends to stabilize, thus reflecting the permeable nature of the system.

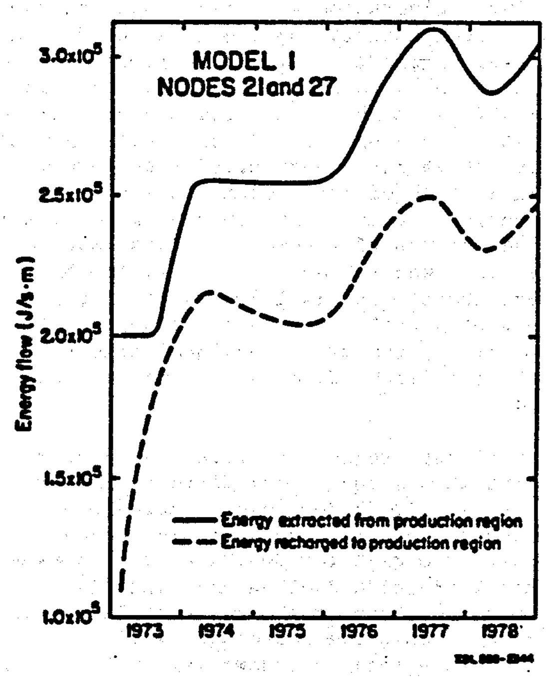

Figure 21. Model 1. Energy extracted and recharged to the production region (nodes 21 and 27).

It is of interest to examine the cause of the pressure declines in the α reservoir. In most cases, reservoir pressure reduction is attributed to density changes due to limited recharge. However, as shown in Figure 23, results for Model 1 show that the recharge rate is generally higher than the extraction rate during the simulation. Thus, the pressure reduction is primarily caused by fluid contraction because of the temperature decline.

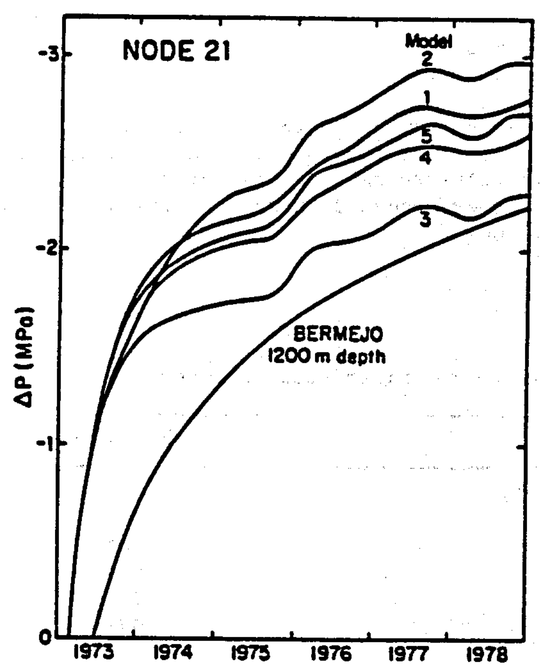

Figure 22. Pressure changes in node 21 for the five models studied under exploitation ($Q = Q_T/3000$ m).

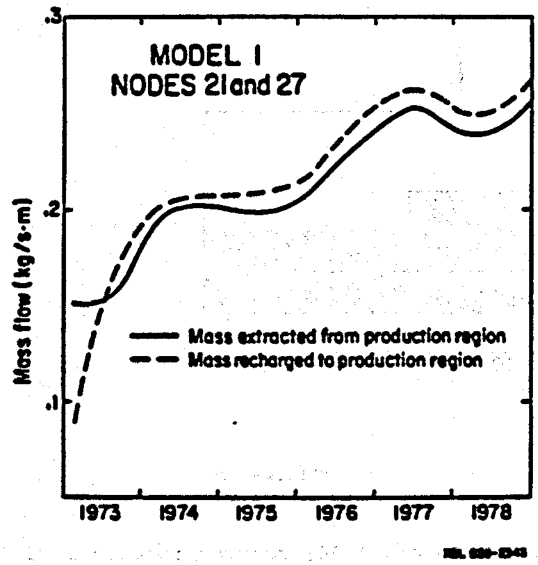

Figure 23. Model 1. Mass extracted and recharged to the production region (nodes 21 and 27).

In all cases, the initial pressure drop is much larger than that of Bermejo et al. (1979). This could be explained by the two-dimensional nature of the model which does not allow for recharge from all directions, and does not take into account the presence of CO_2 in the reservoir fluids. The latter factor enhances boiling in the reservoir by lowering the boiling temperature of the water. Assuming a 0.5% (by mass) of CO_2 in the Cerro Prieto fluids, and using Henry's law, the partial pressure of CO_2 at 300°C is estimated as 0.55 MPa.

A more extensive two-phase zone in the reservoir caused by the presence of CO_2 would significantly increase the compressibility of the system and consequently slow down the pressure reduction. Therefore, it is possible that the computed initial pressure decline is too large because the effects of noncondensable gases were neglected.

Figures 24 to 32 show the pressure changes, temperature changes and mass flow patterns at the end of 1978 for Models 1, 3, and 5. Simulation of production after 1978 was not carried out due to a lack of data on the pressure history of the α reservoir and because at that time new wells, located in the southwestern and eastern part of the field, were put on line. Consequently, we feel that only a model that considers the three dimensional nature of the geology and of the flow pattern is appropriate for simulating the behavior of the reservoir after 1978. The development of a three-dimensional model of the field is one of our future objectives.

Figures 24 to 32 illustrate the importance of the western boundary and the fault located between wells M-25 and M-29 in the recharge of the produced α reservoir. For example, in Model 5 at the end of 1978, 86% of the recharge into nodes 21 and 27 (representing the α reservoir under exploitation) comes from the west and the fault, 5% from the east and the vertical gap between the shaly units, 6% from the underlying layer, and the remaining 2% from the overlying layer.

The presence of the two-phase zone in the vertical gap which connects the α and β reservoirs, the associated mobility decrease due to relative permeability effects, and the low vertical permeability, limit the mass recharge to the α reservoir from deeper parts of the system.

Some authors (Bermejo et al., 1979 and Sánchez and de la Peña, 1981) have suggested that there is significant recharge to the α reservoir from the east (e.g. see Figure 9). The results of our modeling studies indicate that a very small fraction of the recharge comes from that direction. Our work, in agreement with that of other authors (e.g., Fausto et al., 1981; Grant et al., 1981) indicates that most of the recharge to the α reservoir comes from the west and from shallower zones.

Because of the high permeability of the system, the extent of the two-phase zones increases only slightly, or not at all, in our simulations during exploitation. Furthermore, no boiling occurs in the production nodes located in the α reservoir. This agrees with the findings of Grant et al. (1981) that boiling occurs only near the wells and that no extensive two-phase zone has developed in the α reservoir during exploitation.

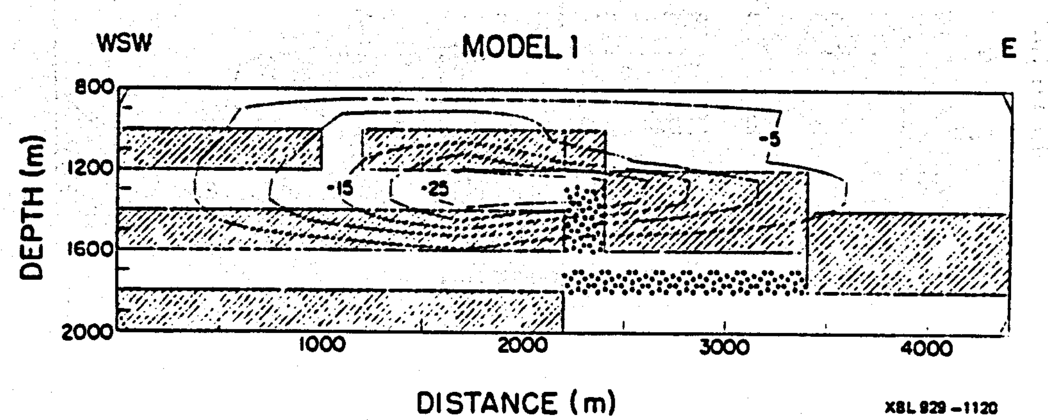

Figure 24. Model 1 - Exploitation. Pressure changes between 1973 and 1978; contour interval: 5 bars (0.5 MPa).

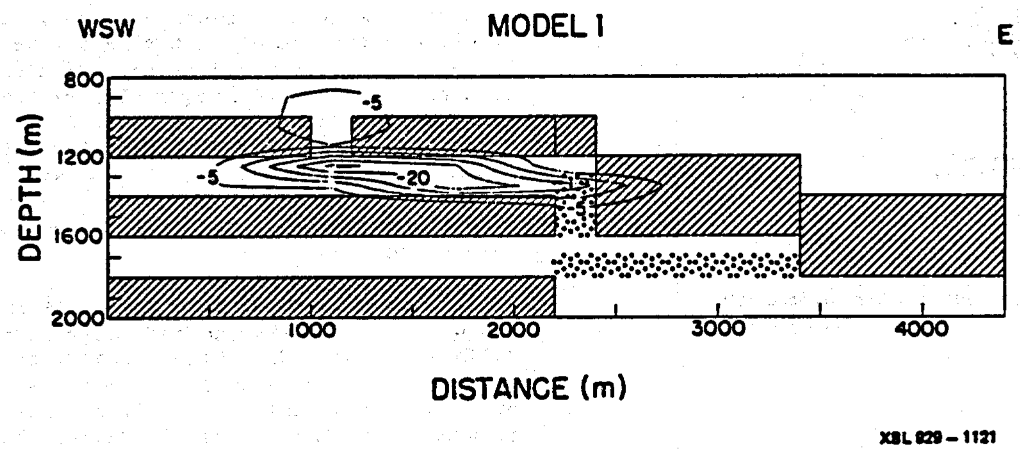

Figure 25. Model 1 - Exploitation. Temperature changes between 1973 and 1978; contour interval: 5°C.

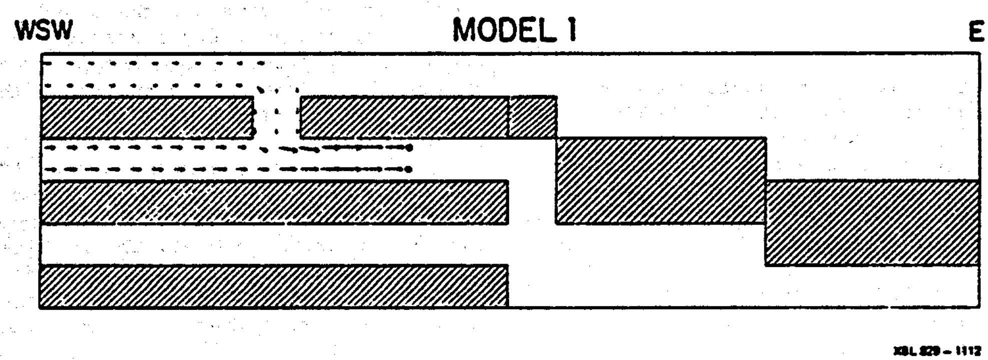

Figure 26. Model 1 - Exploitation. Mass flow pattern at the end of 1978. The two dots indicate where the fluids are extracted from the system.

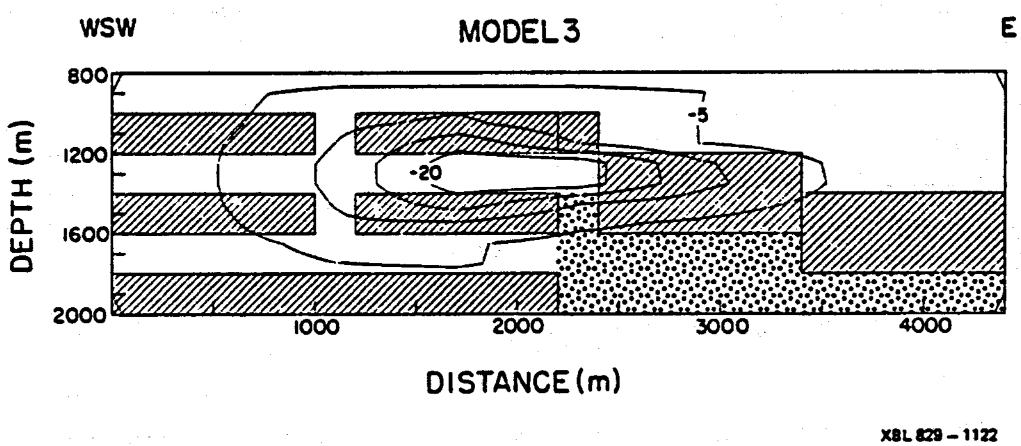

Figure 27. Model 3 - Exploitation. Pressure changes between 1973 and 1978; contour interval: 5 bars (0.5 MPa).

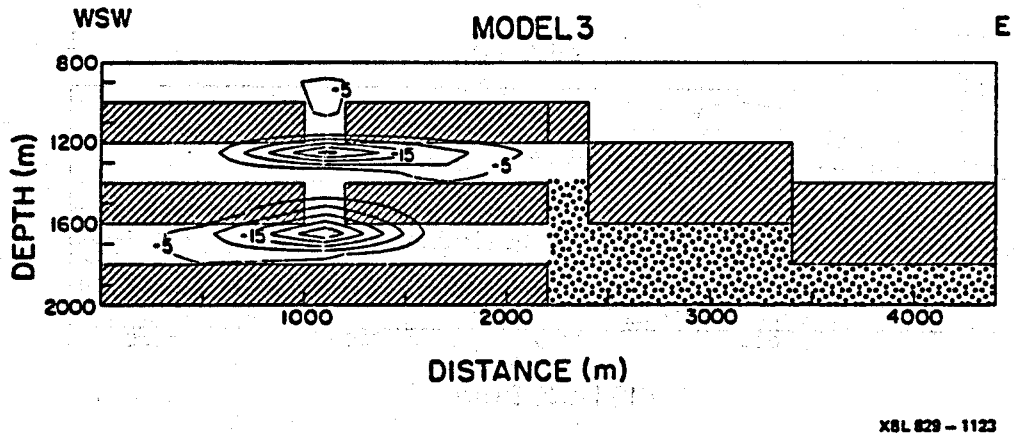

Figure 28. Model 3 - Exploitation. Temperature changes between 1973 and 1978; contour interval: 5°C.

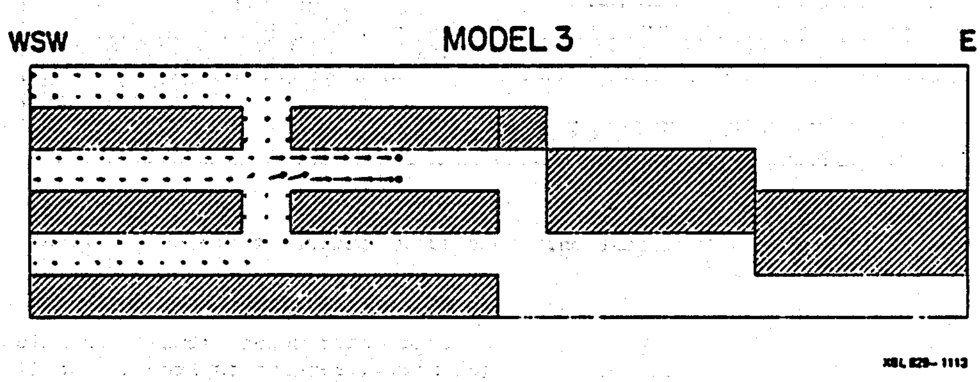

Figure 29. Model 3 - Exploitation. Mass flow pattern at the end of 1978.

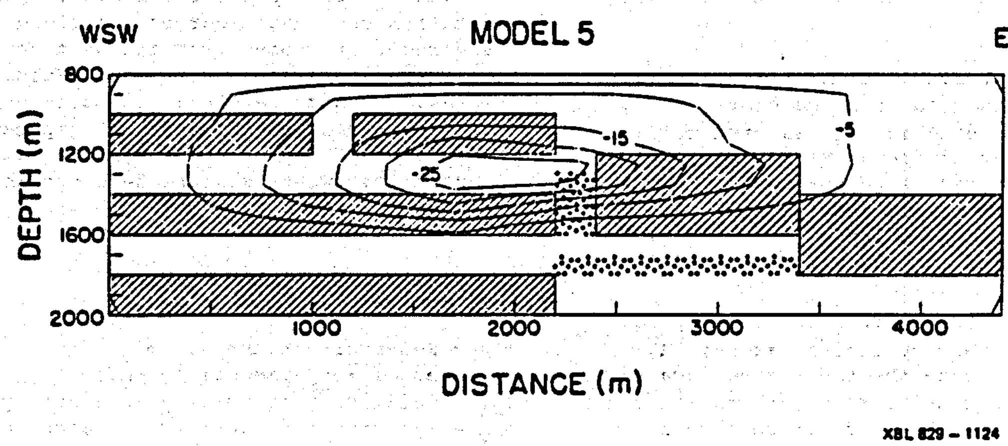

Figure 30. Model 5 - Exploitation. Pressure changes between 1973 and 1978; contour interval: 5 bars (0.5 MPa).

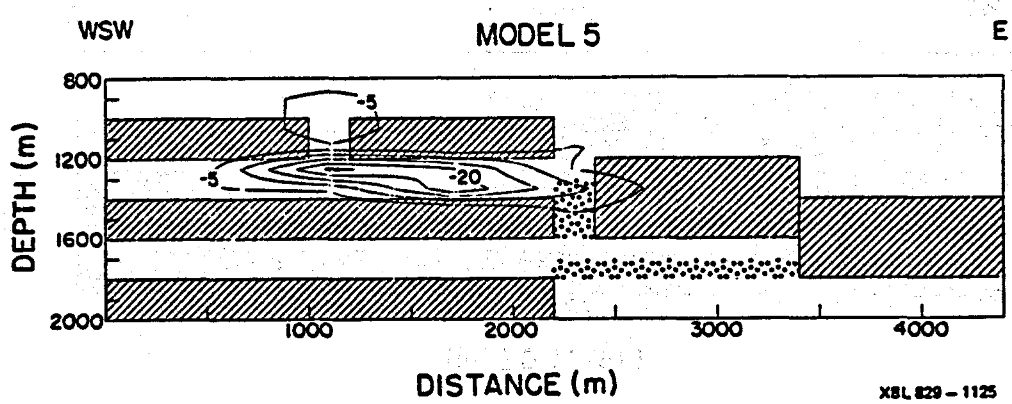

Figure 31. Model 5 - Exploitation. Temperature changes between 1973 and 1978; contour interval: 5°C.

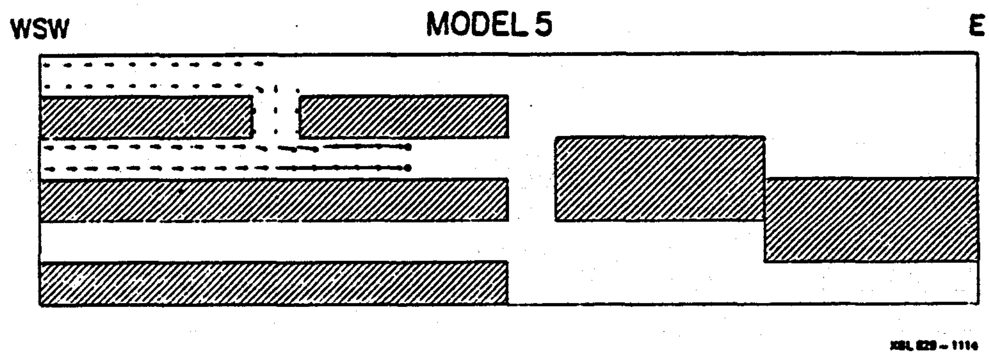

Figure 32. Model 5 - Exploitation. Mass flow pattern at the end of 1978.

CONCLUSIONS

The results of the studies on the natural state of the Cerro Prieto field and the studies of the reservoir behavior under exploitation indicate that Models 1, 4 and 5 best match measured values. All of these models agree well with observed data, so that at the present time one cannot decisively single out any one model as the best. However, the physical differences between the three models are small.

The results indicate that the field in its natural state is recharged from the east with hot water (about 10^{-2} kg/s·m) as well as with colder waters from shallower aquifers, especially from the west. The hot waters flow upwards through a vertical gap in the shaly layers (east of well M-10) and move into the western α and β reservoirs. Some boiling occurs as the hot waters ascend.

The α reservoir is fed from the east by hot waters and from the west by cooler waters. As these waters move towards the fault zone located between wells M-25 and M-29, they tend to mix and then flow upwards through the fault zone to a shallow aquifer. This shallow aquifer discharges to the west and the water eventually feeds the surface manifestations at the western region of the field.

Mineral deposition or self-sealing of the porous sediments could explain the minimal influx of cold water under natural conditions into the geothermal reservoirs from the shallow aquifer overlying the system. The results show that the fault between wells M-25 and M-29 does not permit much fluid flow between the α and β reservoirs, but does connect the α reservoir with the shallow aquifer.

Our studies of the reservoir response to exploitation show that most of the fluid recharge to the α reservoir comes from the west and from shallow layers above the fault zone. Recharge from the east seems to be minor due to the presence of a two-phase zone in the vertical gap between the shaly layers. Because of the large fluid recharge, no extensive two-phase zone develops in the α reservoir.

NOMENCLATURE

h = Reservoir thickness (m)
k = Absolute permeability (md)
k_{rl} = Relative permeability of liquid phase
k_{rv} = Relative permeability of vapor phase
P = Pressure (Pa)
Q = Flow rate (kg/s·m)
Q_T = Total flow (kg/s)
S = Vapor saturation
S_{rl} = Residual (immobile) liquid saturation
S_{rv} = Residual (immobile) vapor saturation
ϕ = Porosity

ACKNOWLEDGEMENTS

We wish to thank our colleagues at the U.S. Geological Survey and the Lawrence Berkeley Laboratory for stimulating discussions, in particular Alfred Truesdell (USGS), Susan Halfman (LBL) and Karsten Pruess (LBL). We want to thank Mark Sluka, Marilee Bailey and Christine Doughty for preparing the illustrations and Aylette Villemain for typing the manuscript.

This work was supported by the Assistant Secretary for Conservation and Renewable Energy, Office of Renewable Technology, Division of Geothermal and Hydropower Technologies of the U. S. Department of Energy under Contract Number DE-AC03-76SF00098.

REFERENCES

To avoid monotonous repetitions, the proceedings of the symposia on Cerro Prieto will be referenced using the following abbreviations:

CPI: Proceedings of the First Symposium on the Cerro Prieto Geothermal Field, September 20-22, 1978, San Diego, California. Lawrence Berkeley Laboratory report LBL-7098.

CPII: Proceedings of the Second Symposium on the Cerro Prieto Geothermal Field, October 17-19, 1979, Mexicali, Baja California, Mexico. Comisión Federal de Electricidad.

CPIII: Proceedings of the Third Symposium on the Cerro Prieto Geothermal Field, March 24-26, 1981, San Francisco, California. Lawrence Berkeley Laboratory report LBL-11967.

Abou-Sayed, A.S., J.F. Schatz, and K.M. Wolgemuth, 1979. Compaction and permeability of Cerro Prieto Cores: A Laboratory Evaluation. CPII, pp. 263-268.

Abril G., A. and C. Vargas G., 1981. Resultados de las últimas pruebas transitorias de presión en pozos de Cerro Prieto. CPIII, pp. 504-509.

Bermejo M., F.J., F.X. Navarro O., F. Castillo B., C.A. Esquer and C. Cortez A., 1979. Variación de presión en el yacimiento de Cerro Prieto durante su explotación. CPII, pp. 473-493.

Castillo B., F., F.J. Bermejo M., B. Domínguez A., C.A. Esquer P., and F.J. Navarro O., 1981. Distribución de temperaturas en el campo geotérmico de Cerro Prieto. CPIII, pp. 474-482.

Elders, W.A., A.E. Williams, and J.R. Hoagland, 1981. An integrated model for the natural flow regime in the Cerro Prieto hydrothermal system based upon petrological and isotope geochemical criteria. CPIII, pp. 102-109.

Fausto L., J.J., M.E. Jiménez S., and I. Esquer P., 1981. Estado actual de los estudios sobre geoquímica hidrotermal en Cerro Prieto. CPIII, pp. 188-212.

Grant, M.A., A.H. Truesdell, and A. Mañón M., 1981. Production-induced boiling and cold water entry in the Cerro Prieto geothermal reservoir indicated by chemical and physical measurements. CPIII, pp. 221-237.

Halfman, S.E., M.J. Lippmann, R. Zelwer, and J.H. Howard, 1982. Fluid flow model of the Cerro Prieto geothermal field based on well log interpretation (this volume).

International Formulation Committee, 1967. A formulation of the thermodynamic properties of ordinary water substance. IFC Secretariat, Dusseldorf, West Germany.

Lyons, D.J. and P.C. van de Kamp, 1980. Subsurface geological and geophysical study of the Cerro Prieto geothermal field, Baja California, Mexico. Lawrence Berkeley Laboratory report LBL-10540.

Martínez B., L.F., 1978. Thermal conductivity of core samples from the Cerro Prieto geothermal field: Experimental results and an improved prediction method. CPI, pp. 342-351.

Mercado G., S., 1968. Localización de zonas de máxima actividad hidrotermal por medio de proporciones químicas, campo geotérmico de Cerro Prieto, B.C., presented at the III Congreso Mexicano de Química Pura y Aplicada, March 21-23, 1968. Guadalajara, México. Sociedad Química de México.

Mercado G., S., 1976. Migración de fluidos geotérmicos y distribución de temperaturas en el subsuelo del campo geotérmico de Cerro Prieto, Baja California, México. Proceedings, Second United Nations Symposium on the Development and Use of Geothermal Resources, San Francisco, California, May 20-29, 1975, pp. 487-492.

Prian C., R., 1981. Velocidad de perforación de la secuencia estratigráfica del área de Cerro Prieto. CPIII, pp. 77-84.

Pruess, K. and R.C. Schroeder, 1980. SHAFT79 user's manual. Lawrence Berkeley Laboratory report LBL-10861.

Rivera R., J., F. Samaniego V., and R.C. Schroeder, 1978. Pressure transient testing at the Cerro Prieto geothermal field. CPI, pp. 366-371.

Sánchez R., J. and A. de la Peña L., 1981. Geohidrología del acuífero geotérmico de Cerro Prieto. CPIII, pp. 309-323.

Schatz, J.F., 1981. Properties of Cerro Prieto rock at simulated in-situ conditions. CPIII, pp. 292-296.

Schroeder, R.C., C.B. Goranson, S.M. Benson, and M.J. Lippmann, 1978. Well interference tests at the Cerro Prieto geothermal field. CPI, pp. 357-362.

Somerton, W.H., 1978. Some physical properties of Cerro Prieto cores. CPI, pp. 333-338.

Stanford University, 1980. Proceedings, special panel on geothermal model intercomparison study. Stanford Geothermal Program report SGP-TR-42.